Non-Linear Analysis of Pullout Tests on Inflatable Anchors in Sand

Y. Liang, S. D. Hinchberger, and T. A. Newson
Geotechnical Research Centre, Department of Civil and Environmental Engineering, The University of Western Ontario, London, Ontario, Canada

ABSTRACT
This paper describes the non-linear finite element (FE) analysis of pullout tests of an inflatable anchor embedded in dry sand. The inflatable anchor, which has offshore applications, comprises an anchor rod connected to an inflatable membrane. The pullout resistance is enhanced by inflating the flexible membrane after anchor installation. Scaled model pullout tests were performed in a steel container using different inflation pressures and embedment depths. The results are interpreted using geometric nonlinear FE analyses, which accounts for the non-linear stress-strain behaviour of the sand and flexible membrane. The nonlinear response of the sand is modeled using (i) linear elasticity and the Mohr-coulomb failure criterion and (ii) a nonlinear strain hardening elastoplastic model. The FE analyses illustrate the relative importance of geometric and material nonlinearity when modelling the pullout of this type of anchor.

RÉSUMÉ
Ce papier décrit l'analyse numérique non linéaire de tests de retrait a exécuté sur un ancre gonflable enfoncé dans le sable sec. L'ancre gonflable comprend une tringle d'ancre connectée à une membrane gonflable. La résistance de retrait est améliorée en gonflant la membrane après l'installation d'ancre. Les tests de retrait modèles gradué ont été exécutés dans un récipient en acier utilisant les pressions d'inflation différents et les profondeurs d'embedment. Les résultats sont interprétés utilisant géométrique non linéaire numérique analyse, qui représente le comportement de tension-tension non linéaire du matériel de sable et membrane. Pour le sable, la réponse non linéaire est modelée l'utilisation (je) une élasticité linéaire a couplé avec le modèle de Mohr-coulomb et (II) une tension non linéaire durcit le modèle d'elastoplastic. Le numérique analyse illustrer l'importance de non-linéarité géométrique et matérielle en modelant ce système d'ancre.

1 INTRODUCTION

Temporary anchors are widely used during offshore activities to provide support for temporary structures or to anchor underwater construction equipment. Recently, inflatable anchors have been considered for this application. As illustrated in Fig. 1, an inflatable anchor comprises: (a) an anchor rod, which is attached to (b) an inflatable membrane or packer of length, L, and radius, r_o. The pullout capacity of the anchor is enhanced by inflating the membrane after installation in soft marine sediments. In Fig. 1, H is the embedment depth.

Recently, Newson et al. (2009) studied the response of inflatable anchors in sand using: (i) scaled model pullout tests and (ii) small-strain elastoplastic finite element (FE) analysis to interpret the pullout response. Their study found that the pullout capacity of an inflatable anchor is a function of the embedment depth, H, effective friction angle, inflation pressure and effective anchor length, L_e, of the anchor which is less than the physical length, L (see Fig. 1). In some cases, back analysis of the pullout tests indicated that only 45% of the anchor length was active in developing the pullout capacity. Based on the FE analyses, Newson et al. (2009) hypothesized that the effective length of the anchor, L_e, was less than its physical length, L, due to the deformable nature of the membrane (i.e. large membrane distortions prevented the bottom of the membrane from slipping relative to the soil). However, this hypothesis was based on analyses that: (i) did not consider geometric non-linearity; (ii) considered the soil to be linear elastic prior to failure; and (iii) treated the polymer membrane as a linear elastic material. The objective of this paper is to assess the extent to which non-linear material behaviour and geometric non-linearity affects the pullout response of these anchors.

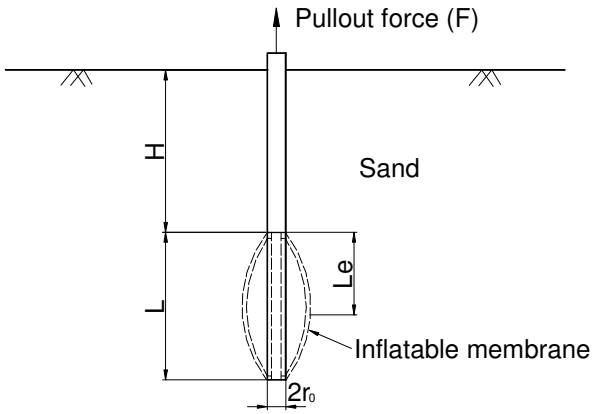

Fig. 1. Inflatable anchor.

First, this paper describes a series of scaled physical model pullout tests conducted on an inflatable anchor embedded in dry sand. The pullout tests were performed in a steel cylindrical container that was filled with air-dried loose sand and thus represents a fully drained condition. Pullout tests were performed on anchors installed with various embedment depths, and inflation pressures. Next, the measured pullout response is interpreted using

the finite program ABAQUS V6.8 (ABAQUS Manual 2003). Full geometric non-linear analyses were performed and the stress-strain response of the sand was modelled using either: (a) linear elasticity coupled with Mohr Coulomb plasticity; and (b) the Lade single hardening constitutive model (Lade et al.1987), which accounts for the non-linearity stress-strain response prior to failure. The inflatable membrane was modeled using a nonlinear hyper-elastic model. Finally, the paper concludes by summarizing the findings arising from the model tests and FE analyses.

2 PULLOUT TESTS

2.1 Test Set-up

The reduced scale pullout tests were carried out in a cylindrical steel container of 1350mm internal diameter, 1550mm height, and wall thickness of 30mm. The total volume of the container is 1.431m^3. Fig. 2 shows the test set up.

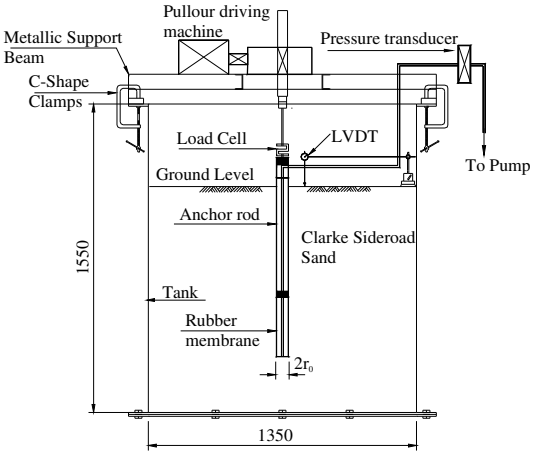

Fig. 2. Pullout test set-up (unit: mm)

A pneumatic controlled piston pump was used to inflate the anchor to the required inflation pressure, p_i. The movement of the pump piston was measured using a LDVT to determine the volume change of the anchor due to inflation. In addition, a pressure transducer was used to measure p_i during each test. Constant p_i tests were performed so the LVDT also provide a measurement of the anchor volume change during pullout.

The anchor was pulled out of the sand filled container using a three-phase motor (Model MC100) attached to a screw jack and 200:1 gear box (see Fig. 2). The motor was computer controlled which allowed different pullout rates to be used, if desired, for each test. In this study, a constant rate of displacement of 0.16mm/min was used for all of the experiments. The axial load was measured using a 1 kN load cell connected in series with the screw jack and anchor head and the load and anchor head displacement were recorded using a computer controlled data acquisition system. Surface heave of the sand was measured during anchor pullout using three LVDTS that where located at distances of 25mm, 220mm and 440mm from the centre of the anchor rod, respectively. However, the surface heave profile is not discussed here.

2.2 Inflatable Anchor

The inflatable anchor, which is illustrated in Fig. 3, comprised a hollow steel anchor rod of diameter of 30mm and length 1000mm. The inflatable portion of the anchor was 300mm long and it comprised a layer of 3.13 mm thick rubber tubing fixed to the rod with compression fittings. The portion of the anchor rod that was covered by the membrane had sixteen 3mm diameter holes drilled in it and the membrane was inflated by pumping fluid through the anchor rod and out of the holes. A small de-airing valve was placed at the end of the anchor rod to remove air.

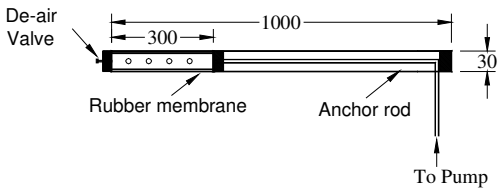

Fig. 3. Inflatable anchor geometry (unit: mm)

2.3 Materials and Properties

The sand used for the pullout tests was obtained from the Lafarge quarry near Clark Sideroad, London, Ontario. Hereafter, the sand will be referred to as C.S. (Clark Sideroad) sand. Grain size analyses were performed on the sand according to ASTM D422. Based on these tests, C.S. sand is medium to fine, brown, angular sand with a coefficient of uniformity C_u = 6 and d_{10}=0.15mm and d_{60}=0.65mm. The specific gravity, G_s, is 2.65.

A series of direct shear tests, and CID triaxial and isotropic triaxial compression tests were performed on loose C.S. sand to determine the engineering properties for the constitutive models. In addition, the sand-to-rubber interface shear strength was measured using a direct shear apparatus. The engineering properties of C.S. sand and the membrane-to-sand interface are summarized in Table 1.

Table 1. Engineering properties of C.S. sand and sand-to-membrane interface.

Void ratio (e)	Density ρ (t/m^3)	Constant Volume Friction Angle, ϕ'_{cv}	Peak Friction Angle, ϕ'_p
0.85	1.58	37.5°	39°
0.45	1.75	37.5°	50°
Interface Friction angle (ϕ')			
Sand-to-membrane		31°	

2.4 Test Sequence

The test sequence for the constant pressure pullout tests was:

i. A steel beam was installed on the top of the test container. This beam was used to hold the anchor in position while placing the C.S. sand.

ii. The anchor was filled with water, de-aired and attached to the beam so that it was centered in the container at the desired embedment depth.
iii. Then, the container was filled in 30cm lifts with C.S. sand until the desired embedment was achieved. The sand was "rained" into place from a sieve that was positioned 130cm above the sand surface at all times. The *in place* density of each lift was measured using small density pots.
iv. After placing the sand, the position beam was removed and a reaction beam was installed and fixed to the container.
v. The pullout motor, screw jack, and load cell were installed in series to the reaction frame and connected to the anchor top.
vi. The inflation pressure was applied in steps using the pneumatic pump.
vii. Finally, the data logger was started, the pullout rate was input into the control software and the test was performed. The pullout force, vertical anchor displacement, volume change and surface heave were investigated during the pullout test.

The above sequence was repeated for all embedment depths and inflation pressures.

3 NUMERICAL ANALYSIS

Two different constitutive models were used to model th stress-strain response of C.S. sand. This sectio provides a brief overview of each model.

3.1 Mohr Coulomb Model

The first model was an elastoplastic model based o linear elasticity and the Mohr-Coulomb failure criterion. I the elastic stress range, the constitutive parameter comprise the Young's modulus, E, and Poisson's ratio, ν, which were both assumed to be constant. Failure was governed by the Mohr-coulomb failure criterion, which is defined by the effective cohesion intercept, c', and friction angle, ϕ'. At failure, a non-associated flow rule was assumed. Thus, the relative magnitude of components of the plastic strain increment vector is governed by the dilation angle, $\phi' \neq \psi$. The constitutive parameters used for the Mohr-Coulomb model are listed in Table 2.

Table 2. Mohr-Coulomb Constitutive Parameters

Young's Modulus, E (kPa)	Poisson's Ratio, ν	Effective Friction Angle, ϕ'	Dilation angle, ψ	Cohesion Intercept, , c' (kPa)
5500	0.3	37.5°	0.5°	0.1

3.2 The Lade Single Hardening Model

The second model used was Lade's model (Lade et al. 1987). Full details of the Lade's model can be found in the papers by Lade and Nelson (1987) and Lade and Kim (1988). This section provides a brief overview only.

The Lade model is an elastoplastic strain hardening model with a single yield surface that is expressed in terms of stress invariants I_1 [$=\sigma_x + \sigma_y + \sigma_z$] and I_3 [$=\sigma_x \sigma_y \sigma_z + 2\tau_{xy}\tau_{yz}\tau_{zx} - (\sigma_x\tau_{yz}\tau_{zy} + \sigma_y\tau_{zx}\tau_{xz} + \sigma_z\tau_{xy}\tau_{yx})$]. It uses five response functions to define the constitutive behaviour of cohesionless soils. The response functions include: (i) a function to define the pressure dependent elasticity modulus; (ii) the failure criterion; (iii) the yield function; (iv) a plastic work hardening and softening function; and (v) a plastic potential function. The response functions are listed in the Appendix. Fig. 4 shows the failure criterion for Lade's model in principal space and on deviatoric planes, respectively.

The Lade model requires 11 parameters that can be determined from three CID triaxial compression tests and one isotropic compression test. In this paper, the constitutive parameters were estimated by hand from these tests and then used to simulate the response of C.S. sand during CID triaxial compression as a validation exercise. Table 3 summarized the constitutive parameters of Lade's model. Section 3.3 discusses the response of C.S. sand during CID triaxial tests. The Lade model has been implemented into the finite element program (ABAQUS) as a user defined model (UMAT). For more details the reader can refer to Jakobsen and Lade (2002).

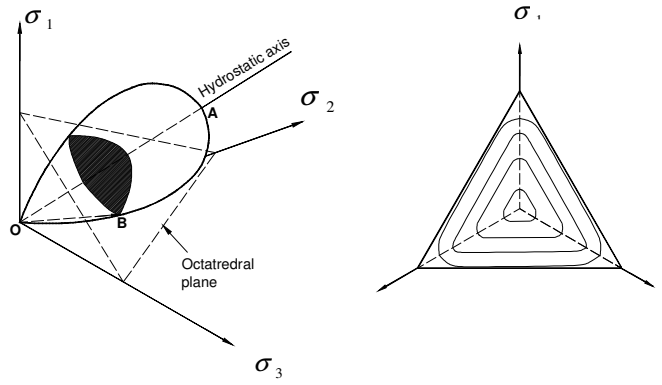

(a) Principal stress space (b) Deviatoric trace

Fig. 4. The failure criterion of Lade's single hardening model

Table 3. Constitutive parameters for the Lade model.

Component	Parameters	Value
Non-linear Elastic Model	M	45
	λ	0.346
	ν	0.2
Failure criterion	m	0.098
	η_1	43
Plastic Potential Function	ψ_2	-3.8
	μ	3.8
Working Hardening–softening region	C	0.005
	p	1.3
Yield criterion	α	0.2
	h	0.98
	ψ_1	See Note

Note: $\psi_1 = 0.00155m^{-1.27}$

3.3 Numerical Validations

3.3.1 Comparison of MC and Lade Models for CID Triaxial Compression.

This section compares the response of C.S. sand during CID triaxial compression tests with the calculated response using (i) the Mohr-coulomb model and (ii) the Lade model.

A two-dimensional axisymmetric FE analysis was performed. The mesh, which is illustrated in Fig. 5, consisted of 54 three-noded linear axisymmetric triangular elements. Linear triangular elements were used since the full contact analysis that was performed to simulate the anchor pullout tests required the use of linear continuum elements for the anchor, membrane and sand. The boundary conditions of the CID finite element mesh were: (i) the vertical component of displacement was fixed (u_z = 0) at the bottom; (ii) the left-hand side of the mesh is a symmetry line (u_x = 0); and (iii) a uniform downward displacement of 1.25cm was applied incrementally to the top surface. A coupled analysis was performed.

In order to simulate the consolidated drained triaxial test, the finite element analyses were carried out in two steps. In the first step, the "geostatic" command was used to define the consolidation stresses and to ensure the model was in equilibrium. Following this step, uniform displacements were applied to the top of the finite element mesh at a very slow rate to ensure that negligible excess po cally sin

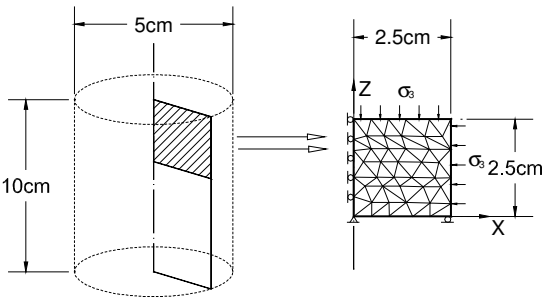

Fig

Fig. 6 compares the measured response of C.S. sand during CID triaxial compression with the calculated response corresponding to: (i) the Mohr-Coulomb model and (ii) the Lade model. From Fig. 6, it is can be seen that finite element results based on Lade's model are very close to the experimental results. From this Figure, it can be seen that C.S. sand exhibits a non-linear stress-strain response from about 25% of the peak deviator stress up to failure. The Lade model is able to simulate this behaviour. In contrast, the Mohr-Coulomb model predicts linear elastic behaviour up to failure followed by perfectly plastic response. Although the deviator stress at failure is predicted satisfactorily, there are significant deviations of the Mohr-coulomb model from the measured response for stresses exceeding about 50% of the peak deviator stress at failure. The consequences of this will become evident in Section 4.

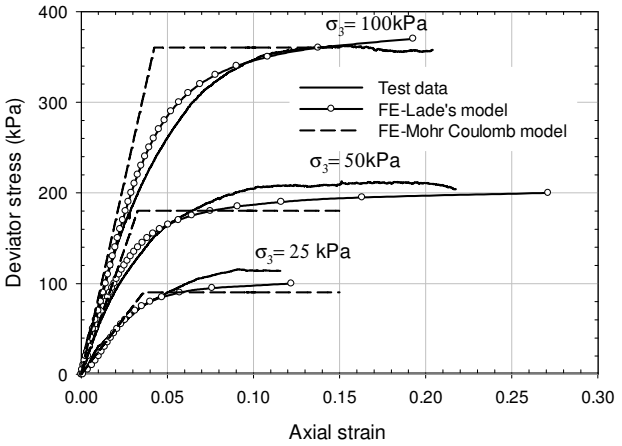

Fig. 6 Comparison of CID behaviour between the FE analysis and the experimental data.

3.3.2 Single Membrane Model

The rubber membrane was modeled as a nonlinear hyper-elastic material. Uniaxial tensile tests were performed to deduce the elastic parameters for the inflatable anchor. Then, an unconstrained membrane inflation test was performed on the inflatable anchor membrane and the test was simulated using ABAQUS and the material parameters deduced from the uniaxial tensile tests.

Fig. 7a shows the axisymmetric FE model used to simulate the unconstrained membrane inflation test. The FE model for unconstrained inflation comprised a membrane of height 300 mm and thickness t=3.3 mm corresponding to the dimensions of the anchor membrane. The membrane was discretized using 80 three-noded linear axisymmetric triangle elements. Rigid fixed boundary conditions were adopted at both ends of the membrane beam and expansion of the membrane was simulated by specifying a uniform horizontal pressure on one side of the membrane that was increased incrementally from 0-80 kPa in 80 steps. A geometric non-linear analysis was performed.

As noted above, the material parameters for the membrane were estimated from the results of uniaxial tensile tests. Hyperelastic polynomial forms can be fitted by ABAQUS up to order *N*=2 using the following energy potential function (ABAQUS manual 2003):

$$U = C_{10}(\overline{I_1} - 3) + C_{01}(\overline{I_2} - 3) + C_{20}(\overline{I_1} - 3)^2 + C_{11}(\overline{I_2} - 3)(\overline{I_2} - 3) + C_{02}(\overline{I_2} - 3)^2 + \sum_{i=1}^{2} \frac{1}{D_i}(J_{e\ell} - 1)^{2i} \quad [1]$$

where U is the strain energy potential, J_{el} is the elastic volumetric strain, $\bar{I}_1$ and $\bar{I}_2$ are the first and second invariants of the strain tensor and C_{10} , C_{01}, C_{20}, C_{11}, C_{02}, D_1 and D_2 are listed below in Table 4. The uniaxial stress-strain response obtained using Eqn. 1 is plotted in Fig. 7b in addition to the measured uniaxial tensile test results. From Fig. 7b, it can be seen that the hyperelastic model matches the uniaxial test data reasonably well. Consequently, the non-linear behavior of the rubber membrane is accounted for; notable, the membrane material becomes stiffer at high strain.

Table 4. Constitutive parameters for the membrane.

D_1	D_2	C_{10}	C_{20}	C_{01}	C_{11}	C_{02}
0	0	-1538	604	2003	-2259	2734

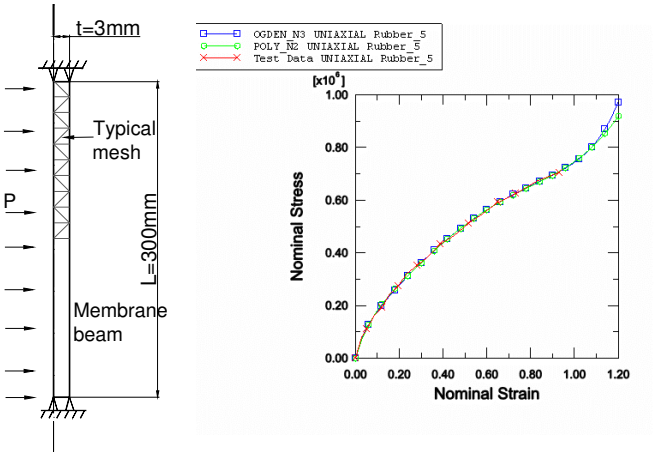

a) FE model b) uniaxial tensile test results

Fig. 7. Unconfined rubber membrane (i) FE model and (b) uniaxial tensile test data.

Fig. 8 shows the calculated and measured inflation pressure (P) versus volumetric strain ($\delta V/V_0$) during unconfined membrane inflation. It can be seen that there is reasonable agreement between the calculated and measured volume change versus inflation pressure for volumetric strains ($\delta V/V_0$) up to 30% using Eqn. 1 for the membrane and material parameters estimated from

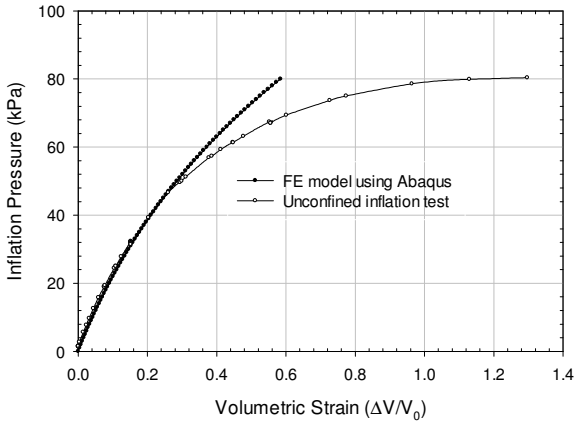

Fig. 8. Experimental versus FE model for unconfined inflation test

3.3.3 FE Model Configuration (Pullout Tests)

Fig. 9 presents a typical FE mesh used for geometric non-linear FE analysis of the anchor pullout tests. The axisymmetric FE model consisted of the anchor shaft, rubber membrane, sand around the anchor and the sand-to-rubber interface. The geometry of the FE model was identical to the physical model test, which is shown in Figs. 2 and 3. Three-noded linear axisymmetric solid triangle elements were used to discretize the sand and rubber membrane. The mesh was finer near the flexible membrane and near the anchor-to-soil interface and it became less fine with distance from the anchor.

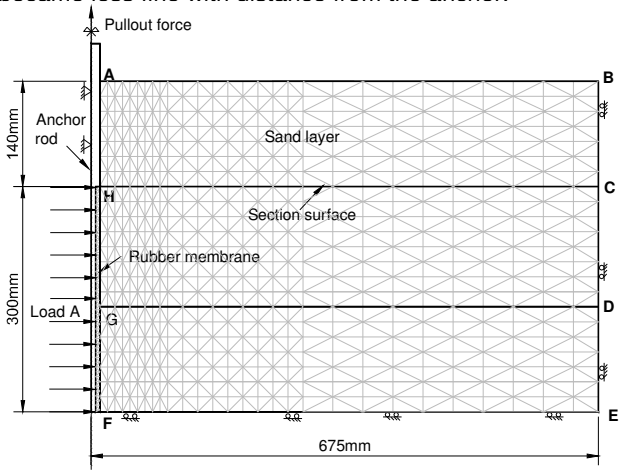

Fig. 9 Typical mesh of inflatable anchor in ABAQUS FE model

Each finite element analysis comprised the following steps: (i) set-up the initial stresses in the sand assuming γ = 15.6 kN/m^3 and K_o = 1.0 for the soil and the anchor (ii) Simulate inflation of the membrane corresponding to the inflation pressures used for each test (see Load A in Fig. 9) and (iii) simulate the pullout by prescribed displacement to the anchor head. The model configuration, material properties and other details of the FE calculations are described below. It is noted that a full geometric non-linear contact analysis was performed wherein master and slave surfaces were defined as discussed below.

The anchor shaft was 35mm diameter and it was modeled as an analytical rigid body assuming no deformation in the test (see ABAQUS User Manual 2003).

The rubber membrane was modeled as a 2nd order polynomial hyperelastic material using the material parameters listed in Table 4. The geometric nonlinear behaviour of the rubber membrane was considered in the analysis

The sand was modeled to the bottom of the anchor only since there is breakaway of the anchor from the soil at this location and other researchers (e.g. Kanakapura et al, 1994) have shown that the soil below the anchor tip has a negligible effect on the pullout response of rigid anchors. In total, 650 elements were used for C.S. sand, which was modelled as either: (i) a linear elastic Mohr-coulomb material using the parameters listed in Table 2; or (ii) a strain-hardening elastoplastic material using Lade's model and the parameters listed in Table 3.

Correct modelling of the anchor-to–sand interface is critical during pullout, especially for situations were separation between the anchor and the surround sand could occur. The contact analysis in ABAQUS uses contact pairs with a master surface and a slave surface. The definitions of the interaction surfaces in this analysis are summarized in Table 5 and described in the following: (i) For the anchor rod-to-sand interface, the analytical rigid body surface was chosen as the master surface and the surrounding soil surface as the slave surface. This

surface was defined as a smooth frictionless surface. (ii) For rubber membrane-to-sand interface, the sand surface was the master surface and the rubber membrane was the slave surface. Based on the direct shear tests performed on the rubber membrane-to-sand interface, the internal friction angle is $\phi' = 31^o$ and consequently the friction penalty method was employed using μ=0.6 (μ=tanϕ').

Table 5. Summary of the interactions used in the FE model

Surface Setting	Anchor Rod-to-Sand		Sand-to-Rubber	
	Master Surface	Slave Surface	Master Surface	Slave Surface
	Anchor	Sand	Sand	Rubber
Contact property	Frictionless		Coulomb friction formulation	
Tangential behaviour			Penalty u=0.6	
Normal behaviour	Hard contact		Hard contact	

4 RESULTS

In this section, the results obtained from the FE calculations are compared with the results of the reduced-scaled laboratory pullout tests.

4.1 Cavity Expansion Response

Fig. 10 shows the relationship between the volume change and the inflation pressure during inflation of the anchor (cavity expansion) corresponding to an anchor embedment depth of H=140mm. It can be seen that the results obtained from the FE analysis using the Lade model agree very well with the laboratory test data with the inflation pressure of P=60kPa before pullout. The Mohr-coulomb model underestimates the amount of

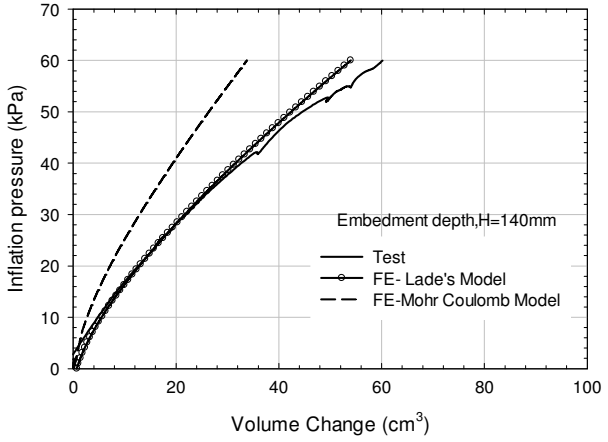

Fig. 10. Comparison of the volume change versus the inflation pressure during the cavity expansion in C.S. sand (H=140mm)

4.2 Pullout Response

Fig. 11 summarized the measured and calculated pullout force versus anchor displacement corresponding to a constant inflation pressure of 60kPa and embedment depths of 140mm, 300mm and 550mm, respectively. From this Figure, it can seen that the peak pullout force, P_{ult}, increases with embedment depth, which is to be expected. The P_{ult} is 480N for H=550mm and 170N for H=140mm. The corresponding displacement at P_{ult} is 10mm for H=140mm, 12mm for H=300mm and 38mm for H=550mm.

The calculated pullout force versus displacement curves obtained from FE analysis are plotted as solid and dashed lines in Fig. 11. The solid lines correspond to the Lade model and the dashed lines to the Mohr-coulomb model. The following observations can be made by comparing the measured and calculated behaviour:

i. First, FE calculations using the Mohr-coulomb model result in underestimation of the displacement at P_{ult}. There is better agreement between calculated and measured response using the Lade model.
ii. The Lade model predicts more nonlinearity prior to the peak pullout force; whereas, the Mohr-coulomb model predicts less non-linearity. Thus, accounting for the non-linear stress-strain response of C.S. sand leads to better agreement between the calculated and measured load-displacement response.
iii. The FE analysis using the Lade model predicts decreasing pullout force with displacement after reaching P_{ult} similar to that seen in the experiments. In contrast, the Mohr-coulomb model does not. This is attributed to the constant dilation

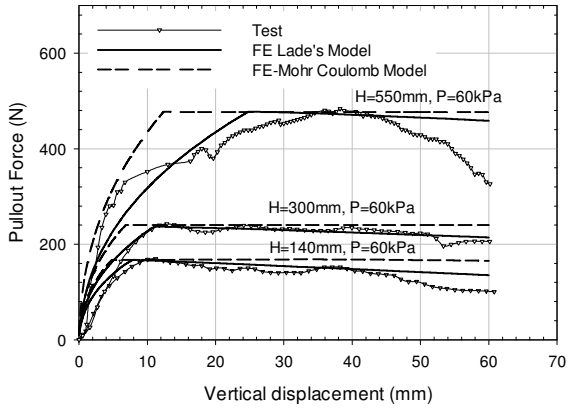

Fig. 11. Comparison of the pullout force versus anchor displacement with changing the embedment depth

Fig. 12 summarizes the measured and calculated pullout force versus anchor displacement for a constant embedment depth of 140mm and inflation pressures, p_i, of 0, 60 and 80kPa, respectively. As expected, P_{ult} increases with increasing p_i and H. In this case, P_{ult} increases from 92N corresponding to zero inflation pressure to 208N for an inflation pressure of 80kPa. Thus, the inflation pressure has a significant impact on the anchor capacity.

In Fig. 12, the calculated P_{ult} is comparable to the measured P_{ult} for both constitutive models for the various inflation pressures. As a result, it can be concluded that both the Mohr-coulomb and Lade models are able to simulate the peak pullout force versus inflation pressure of the anchors. However, similar to that seen above in Fig. 11, the calculated load-displacement response prior to failure is better for the Lade model compared to the Mohr-coulomb model, which can be attributed to the non-linear stress-strain behaviour of the Lade model (see Fig. 6). Finally, FE analysis using Lade's model is able to predict the decrease in pullout force versus displacement after reaching P_{ult}. This is thought to be due to the constant dilation angle used in the Mohr-coulomb model compared to [illegible] del

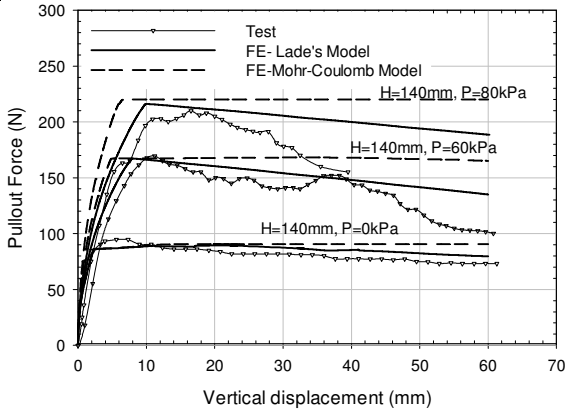

Fig. 12. Comparison of the pullout capacity versus anchor displacement with various inflation pressures

4.2.1 Evaluation of the Effective Length, L_e

As discussed above, Newson et al. (2009) deduced that the pullout response of inflatable anchors is dependent on the effective anchor length, which is less than the physical length of the membrane (see Fig. 1). In order to investigate this, Figs. 13-15 show contours of calculated vertical and horizontal stresses in the C.S. sand adjacent to an anchor with H=140mm, and p_i=60 kPa. In addition, from Newson et al. (2009), the effective length corresponding to this anchor is 0.45L, which is less than half of the physical length of the membrane.

Referring to Fig. 13, it can be seen that there are two distinct trends in terms of the vertical stress field around an inflatable anchor: (i) First, there is a significant increase in the vertical stress at about the midpoint of the anchor. This is roughly consistent with the effective length zone. (ii) Second, there is a corresponding decrease in vertical stress around the lower portion of the anchor, which is due to anchor separation as discussed below. At the anchor bottom, the stresses are close to zero, which would account for the negligible shear resistance offered by the lower portion of the anchor.

Figs. 14 and 15 show contours of the calculated horizontal stresses in the C.S. sand after membrane inflation (p_i=60kPa) and at P_{ult}, respectively. From Fig. 14, it can be seen that the horizontal stresses around the anchor after inflation are relatively uniform along the anchor length and they dissipate with distance from the anchor, which is consistent with cavity expansion solutions. The maximum horizontal stress is about 22kPa on the membrane-to-sand interface corresponding to p_i=60kPa. Thus, about 38kPa of the internal inflation pressure, p_i, is resisted by the membrane and only 22kPa by the sand.

At P_{ult} (see Fig. 15), however, there is significant reduction of the horizontal stresses in the sand at the anchor top and bottom. The decrease in stress at the anchor bottom is caused by anchor-soil separation as illustrated by the displaced position of the anchor in Fig. 15. In contrast, the reduction of horizontal stress at the anchor top is a caused by soil-structure interaction between the non-linear membrane and the sand. During pullout, tensile force is transferred to the upper portions of the membrane. Based on the FE analysis, this increases the stress in the membrane causing it to stiffen (see Fig. 7). Consequently, at P_{ult} the stiffened membrane carries a greater proportion of the internal inflation pressure and less is transferred to the C.S. sand through the membrane-to-sand interface.

In summary, the above results and discussions confirm the effective length, L_e, concept proposed by Newson et al. (2009). However, based on the nonlinear FE analysis, the effective length of the anchor is less than that deduced by Newson et al. (2009) and it is situated near the midpoint of the anchor (see Figs. 13 and 15).

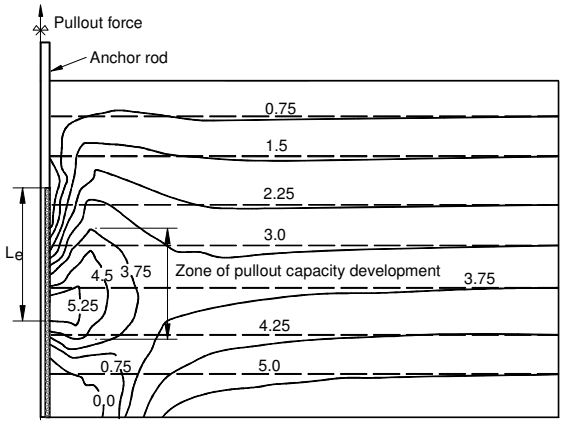

Fig. 13. Vertical stress change around the anchor with the embedment depth of H=140mm

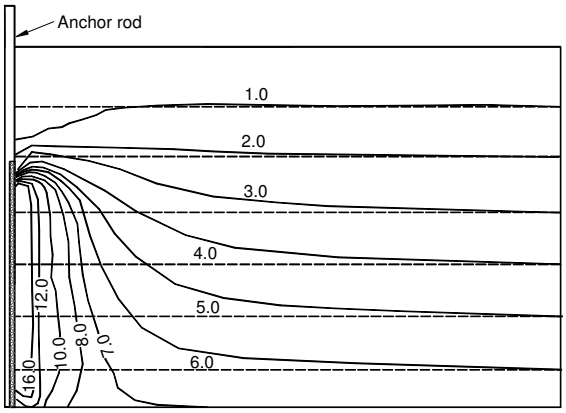

Fig. 14. Horizontal stress change around the anchor just after cavity expansion

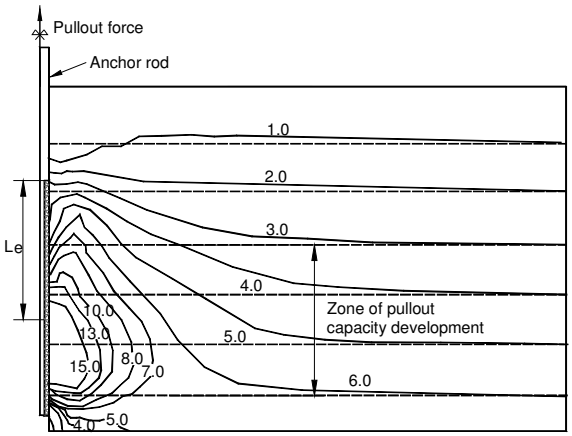

Fig. 15. Horizontal stress change around the anchor with the anchor pullout 20mm

4.3 CONCLUSIONS

This paper has examined the pullout response of an inflatable anchor in dry sand. Based on the above analyses, results and discussions, the following conclusions can be drawn:

1) Pullout tests on inflatable anchors embedded in loose C.S. sand can be adequately modeled using FE analysis accounting for material and geometric nonlinearity.
2) The best agreement between calculated and measured anchor response was obtained when a non-linear strain hardening model was used (Lade et al., 1987); whereas, the analyses using the Mohr-coulomb model were less accurate.
3) Both constitutive models were able to account for the effects of inflation pressure and embedment depth on the ultimate anchor pullout force.
4) Analyses using the Lade model were able to simulate the decrease in anchor pullout load versus displacement after failure. This is attributed to the plastic potential function in the Lade model which reaches constant volume. The Mohr-coulomb model could not simulate this behaviour.
5) The non-linear analysis confirms the concept of an effective length for inflatable anchors, which is less than the physical length of the membrane. In this study, the upper and lower portions of the membrane were found to be ineffective due to stress relief; whereas, the middle zone was effective.

ACKNOWLEDGEMENTS
The research reported in this paper has been funds from NSERC Discovery Grants held by Drs. Hinchberger and Newson. The authors would also like to thank Prof. Lade for providing the user defined routines for ABAQUS.

REFERENCES

Gallacher, T. S. 2000. Novel Anchoring Systems For Remotely Operated Vehicles, Honors Year Dissertation. The 4th year B.Eng thesis. Department of Civil Engineering, the University of Dundee, Scotland, UK.

Hibbit, Karlson and Soresen Inc. 2003. ABAQUS Version 6.5 Manuals.

Jakobsen K. P., Lade, P. V. 2002. Implementation Algorithm for a Single Hardening Constitutive Model for Frictional Materials, International Journal for Numerical and Analytical Methods in Geomechanics., 26:661-681.

Kanakapura, S., Rao, S. and Kumar, J. 1994. Vertical uplift capacity of horizontal anchors. Journal of Geotechnical Engineering, ASCE, 120(7): 1134-1147.

Lade, P.V. and Jakobsen, K.P. 2002. Incrementalization of a single hardening constitutive model for frictional materials. Int. J. Numer. Anal. meth. Geomech, 2002; 26:647-659

Lade, P.V. and Nelson, R.B. 1987. Modeling the elastic behavior of granular materials. International journal for numerical and analytical methods in geomechanics, 11: 521-542

Lade, P.V. and Kim, M.K. 1998. Single hardening plasticity model for frictional materials. Computers and geotechnics, 6, 13-29.

Newson, T.A., Hinchberger, S.D. and Liang, Y. 2009. The mechanics of inflatable anchors in cohesionless soils, Soils and Foundations, V49. No. 3 p409-420.

Newson, T., Hinchberger, S. and Liang, Y. 2007. Detailed Analysis of Inflatable Anchors in Cohesionless Soil, Geotechnical Research Center Report, No. GEOT-05-07, the University of Western Ontario, London , Ontatio, Canada. P35-50.

Newson, T., Bruning, P. and Gallagher, S. 2003. An experimental study of inflatable offshore anchors, ISOPE Conference 2003, Hawaii, Paper #2003-JSC-127.

APPENDIX

This Appendix summarizes the response functions in Lade's model (Lade and Lakobsen 2002).

Pressure Dependent Elastic Modulus

$E=M(p_a)[(I_1/p_a)^2 + 6(J_2/p_a)(1+v)/(1-2v)]^{\lambda}$;
where $p_a = 101.3kPa$

Failure Criterion

$f_n = (I_1^3/I_3 - 27)(I_1/p_a)^m - \eta_1 = 0$

Yield Function

$f_p = [\psi_1 I_1^3/I_3 - I_1^2/I_2](I_1/p_a)^h e^q - f_p''(W_p) = 0$

where $q = \alpha(f_n/\eta_1)/[1-(1-\alpha)(f_n/\eta_1)]$

Plastic Potential Function

$g_p = (\psi_1 I_1^3/I_3 - I_1^2/I_2 + \psi_2)(I_1/p_a)^{\mu}$

Work-hardening Function

$f_p'' = (1/D)^{h/p}(W_p/p_a)^{h/p}$; where $D = C/(27\psi_1 + 3)^{p/h}$